GEOPHYSICAL RESEARCH LETTERS, VOL. 40, 3596–3601, doi:10.1002/grl.50696, 2013

# Verification of velocity-resistivity relationships derived from structural joint inversion with borehole data

M. Moorkamp,[1,2] A. W. Roberts,[3] M. Jegen,[1] B. Heincke,[1] and R. W. Hobbs[3]

Received 14 May 2013; revised 18 June 2013; accepted 24 June 2013; published 23 July 2013.

[1] We present results of three-dimensional joint inversion of seismic, magnetotelluric, and gravity data over a marine salt dome. Such structures are difficult to image with a single method, and our results demonstrate how combining different techniques can yield improved results. More importantly, we examine the reliability of velocity-conductivity relationships derived from structure-coupled joint inversion approaches. Comparison with a seismic reflection section shows that our models match the upper limit of the salt. Furthermore, velocity and resistivity logs from a borehole drilled into the salt dome's flank match, within error, those recovered by the inversion. The good match suggests that the difference in length scale does not have a significant effect in this case. This provides a strong incentive to incorporate borehole data into the joint inversion in the future and substantiates approaches that use the relationships derived from joint inversion models for lithological classification.
**Citation:** Moorkamp, M., A. W. Roberts, M. Jegen, B. Heincke, and R. W. Hobbs (2013), Verification of velocity-resistivity relationships derived from structural joint inversion with borehole data, *Geophys. Res. Lett.*, *40*, 3596–3601, doi:10.1002/grl.50696.

## 1. Introduction

[2] Detailed and reliable imaging of complex geological structures is one of the current challenges in solid earth geophysics. Many questions in earth sciences can only be answered through high-quality models of the Earth's subsurface.

[3] In addition to advancing the utilization of the information content in different geophysical methods, e.g., using the full seismic waveform [e.g., *Abubakar et al.*, 2012], current research also focuses on combining several different geophysical techniques [e.g., *Lelièvre et al.*, 2012]. These approaches take advantage of the strength of each method in resolving different aspects of the same structure while jointly inverting the different data sets in a single numerical algorithm.

[4] Various joint inversion schemes have been successfully applied to different environments [e.g., *Linde et al.*, 2008; *Vermeesch et al.*, 2009]. Broadly, they can be divided into two categories.

[5] The first category consists of schemes using empirical or laboratory-derived relationships between the different types of geophysical parameters. Such approaches are particularly popular for joint inversion of seismic and gravity data, where parameter relationships not only are well established [e.g., *De Stefano et al.*, 2011] but also have been used to couple other types of parameters [e.g., *Heincke et al.*, 2006; *Jegen et al.*, 2009].

[6] Schemes in the second category use a structural constraint that aims at matching the directions of the changes in the different parameters with little or no regard for the magnitude of the change, for example, the cross-gradient approach [*Gallardo and Meju*, 2003].

[7] Parameter relationship-based joint inversion approaches aim at making maximum use of the available information but run the risk of introducing spurious features if the relationship is not valid everywhere in the area under investigation. Conversely, structural approaches are conservative in the sense that they make as few assumptions as possible about relationships between the different geophysical parameters but might not utilize the full potential of joint inversion [*Moorkamp et al.*, 2011].

[8] A currently open question is in how far parameter relationships derived from structural joint inversion correspond to parameter relationships derived from borehole logs and theoretical models [e.g., *Carcione et al.*, 2007]. Previous studies have utilized structural joint inversion to infer velocity-conductivity relationships and constructed lithological classifications based on these relationships [e.g., *Gallardo and Meju*, 2004; *Doetsch et al.*, 2010]. The results are geologically plausible; however, the validity of the relationships has been based on their clustering properties or justified by comparing the relationships from joint inversion of different geophysical data sets [*Gallardo and Meju*, 2007]. Here we provide the first test for structurally derived velocity-conductivity relationships by comparing our structural joint inversion results to borehole logging data from the same area. While this does not provide conclusive proof that structural joint inversion can be used to retrieve parameter relationships under all circumstances, it provides further justification for using such relationships for further analysis and, alternatively, using borehole logging data as a coupling constraint in joint inversion.

## 2. Joint Inversion Method

[9] The theoretical aspects of the joint inversion method, including a detailed comparison of the influence of different coupling approaches on synthetic models, have already been described in *Moorkamp et al.* [2011]. We therefore only give a brief description of the main aspects of our joint inversion framework. We jointly invert seismic first-arrival travel-time data, magnetotelluric impedances, and vertical component

[1]GEOMAR, Helmholtz Centre for Ocean Research Kiel Kiel, Germany.
[2]Now at Department of Geology, University of Leicester, Leicester, UK.
[3]Department of Earth Sciences, Durham University, Durham, UK.

Corresponding author: M. Moorkamp, Department of Geology, University of Leicester, University Rd., Leicester LE1 7RH, UK. (mm489@le.ac.uk)


0094-8276/13/10.1002/grl.50696

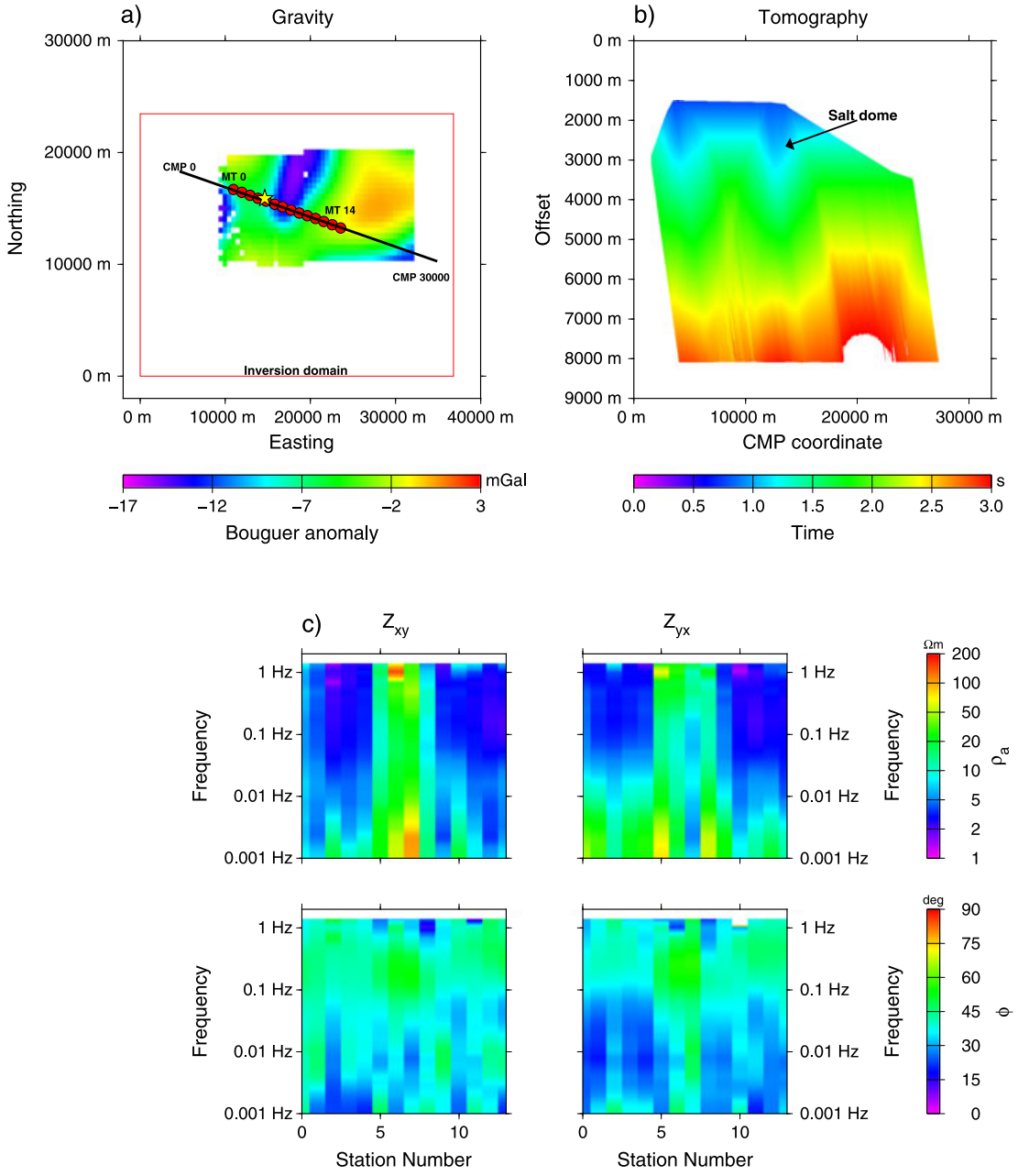


**Figure 1.** Overview of the data sets used for joint inversion. (a) Map view of the gravity data with the inversion domain outlined in red, the seismic transect as a black line, and the magnetotelluric stations as red dots. The yellow star marks the location of two boreholes drilled into the flank of the salt dome. (b) The first-arrival data are displayed as travel time as a function of common midpoint (CMP) and source-receiver offset along the seismic line. (c) Apparent resistivity $\rho_a$ and phase $\phi$ for the two off-diagonal elements $Z_{xy}$ and $Z_{yx}$ of the magnetotelluric impedance tensor.

gravity data for a common three-dimensional model. Our framework allows for a number of different methods to couple the different physical parameters. In this study we use the cross-gradient constraint to enforce interaction. We parametrize our models in terms of seismic slowness $s$, density $\rho$, and conductivity $\sigma$ on a regular grid, and as a result, our objective function $\Phi_{\text{joint}}$ consists of three least squares data misfit terms $\Phi_{\text{d}}$, three cross-gradient constraint terms $\Phi_{\text{cross}}$, and three regularization terms $\Phi_{\text{Reg}}$, viz.,

$$\Phi_{\text{joint}} = \Phi_{\text{d,seis}} + \Phi_{\text{d,grav}} + \Phi_{\text{d,MT}} + \Phi_{\text{cross},s/\rho} + \Phi_{\text{cross},s/\sigma} + \Phi_{\text{cross},\sigma/\rho} + \Phi_{\text{Reg},s} + \Phi_{\text{Reg},\rho} + \Phi_{\text{Reg},\sigma}. \quad (1)$$

Using a limited memory quasi-Newton method [*Nocedal and Wright*, 2006], we iteratively minimize the joint objective function. Within the objective function, we can adjust the relative weighting of the different terms by scaling the variance of the data and the model covariances [*Moorkamp et al.*, 2011].

[10] In order to satisfy specific discretization criteria, we refine the inversion grid separately for each method. We compute first-arrival travel times using the eikonal solver by *Podvin and Lecomte* [1991] and calculate the gradient of the objective function by ray-backtracing through the travel-time solution [*Heincke et al.*, 2006]. Magnetotelluric

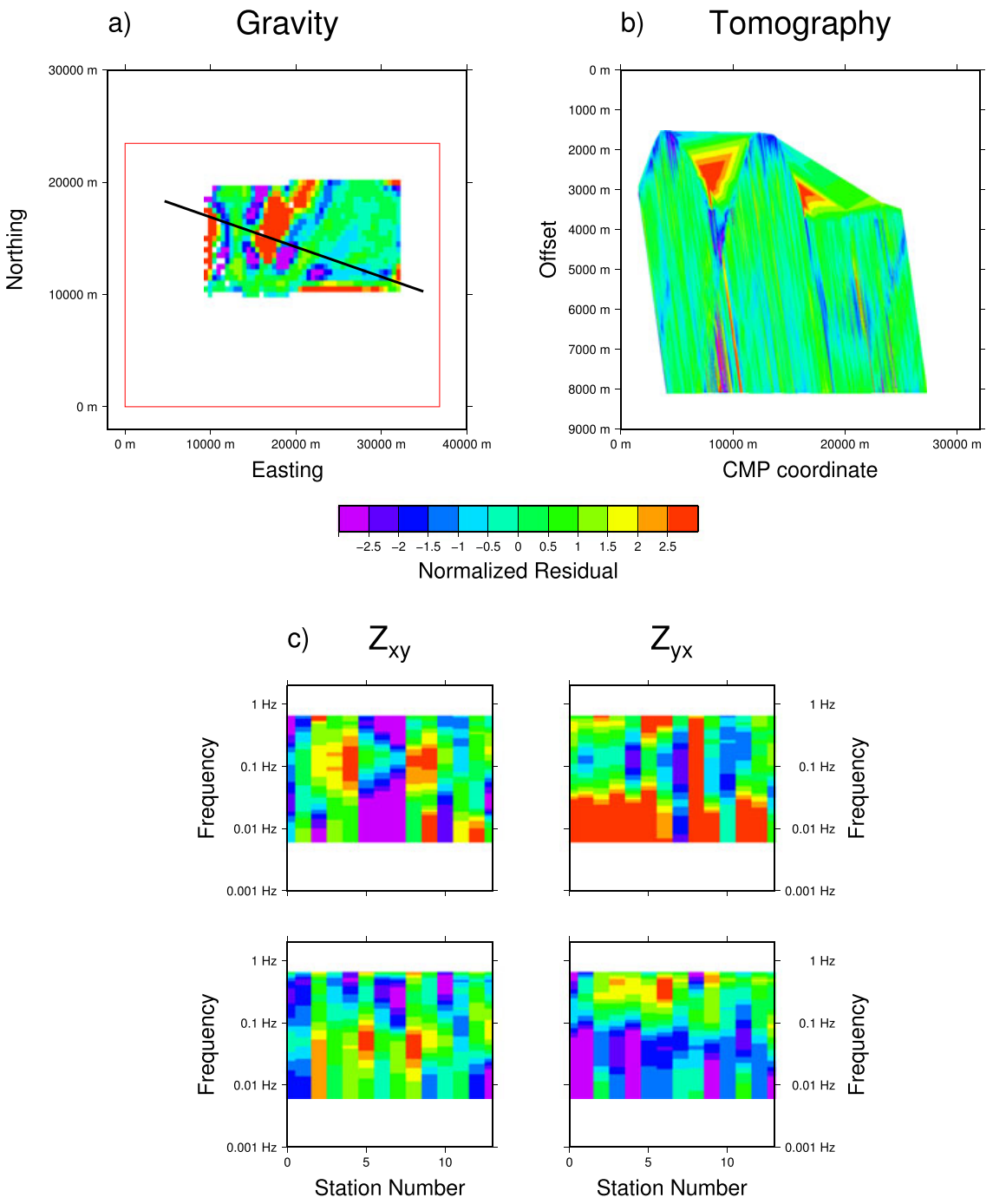


**Figure 2.** Normalized residuals $(d^{obs} - d^{pred})/\Delta d$ of the joint inversion results for the data sets displayed in Figure 1.

impedances and the associated gradient are calculated using the integral equation code by *Avdeev et al.* [2002] and the adjoint method described in *Avdeev and Avdeeva* [2009]. We discuss the detailed aspects of the gravity forward computations in *Moorkamp et al.* [2010].

## 3. Application to Salt Dome Imaging

[11] We apply our joint inversion approach to a data set acquired over a submarine salt dome (Figure 1). Although the gravity data have been measured over the whole area of the salt dome, we only have long-offset seismic and magnetotelluric data measured along a single profile. Thus, even though we are employing a three-dimensional inversion approach, we will only present inversion results below this profile, where we have resolution from all data sets. This is a typical situation with surveys that have not been specifically designed for joint inversion and emphasizes the need for dedicated joint inversion experiments.

[12] All three methods show the influence of the salt dome on the data (Figure 1). We observe a negative Bouguer gravity anomaly in the center of the measurement area, typical for low-density salt within higher-density sediments [e.g., *Nagihara and Hall*, 2001]. The seismic travel times show

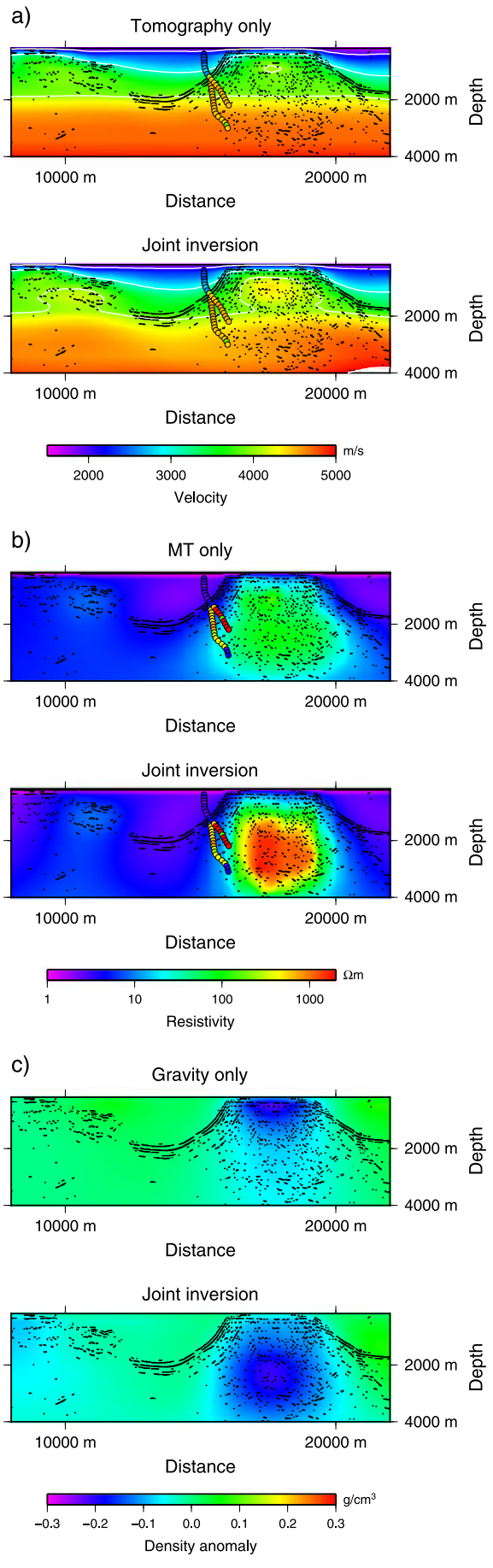


two areas of higher velocity, one corresponding to the salt structure under investigation here (marked in Figure 1b) and a second salt dome outside the area covered by magnetotelluric (MT) and gravity data. Finally, the magnetotelluric data show high apparent resistivities for both off-diagonal elements of the impedance tensor in the center of the profile.

[13] We use an inversion model with 51 × 80 × 16 cells in the north, east, and down directions, respectively. In both horizontal directions, the length of the cells are 460 m throughout the entire inversion domain, while in the vertical direction, the cell size varies between 230 m at the top and 920 m in the deeper parts. The extent of the inversion domain is shown in Figure 1a; it is considerably larger than the extent of the survey area in order to consider effects from lateral structures on the magnetotelluric and gravity measurements.

[14] In the survey area, the seabed is smooth and to a first-order approximation has a constant depth of 230 m. We set seismic velocity and conductivity for the water layer to 1480 m/s and 3 S/m, respectively. The gravity data are Bouguer corrected, and the mean value has been removed, such that we only model anomalous densities. Consequently, the starting model for the density part of the inversion is 0.0 g/cm$^3$ everywhere within the inversion domain. Also, we average all gravity measurements to a spacing of 500 m to make the spacing of the data comparable with the inversion grid, resulting in 913 gravity stations.

[15] For the MT starting model, we use a homogeneous half space with a resistivity of 5 Ωm, and we include all impedance tensor elements at 13 periods between 1.4 and 100 s in the inversion. For the tomography, velocity increases with depth from 2200 m/s at the seafloor to 5500 m/s at a depth of 6 km and we use 384, 353 first-arrival travel-time picks with offsets between 2 and 8 km.

[16] We determine adequate weights for the cross-gradient and regularization terms by experimenting with a range of values and choosing the parameter with the optimum trade-off based on the L-curve criterion [*Hansen*, 1992]. As for the synthetic examples presented in *Moorkamp et al.* [2011], we observe that the exact value of the cross-gradient weight is not critical [see also *Linde et al.*, 2008]. We regularize the inversion by minimizing the curvature of the inversion model. After 370 iterations, we achieve RMS misfits of 0.8, 1.8, and 1.1 for seismic tomography, MT, and gravity data, respectively.

[17] Figure 2 shows the data fits of the joint inversion for all three methods. For the individual inversions, the RMS misfit values are 1.0, 1.9, and 1.0 for seismic tomography, MT, and gravity data, respectively. It is difficult to achieve identical misfits for individual and joint inversion results due to the interaction between the different data sets within the joint inversion and the additional cross-gradient constraints, but these values are similar enough that a different fit to the data does not account for the observed differences in

**Figure 3.** Comparison of (a) seismic velocity, (b) resistivity, and (c) density below the seismic line retrieved from individual inversions and joint inversion. For the seismic velocity and resistivity models, we show the track of two wells drilled into the flank of the salt dome and the associated logging values averaged in intervals of 100 m. On each plot, we also display significant reflections from a migrated seismic section.

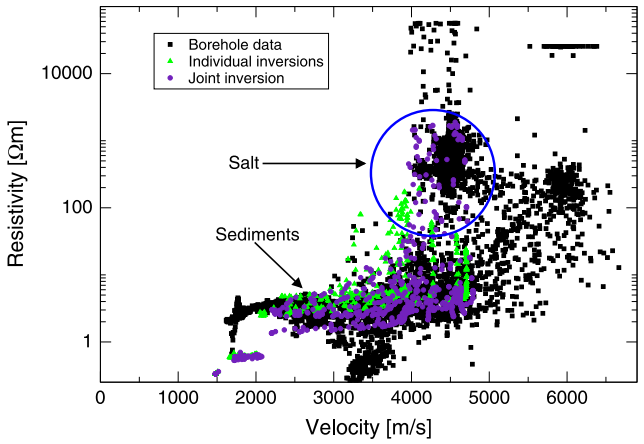


**Figure 4.** Comparison of velocity-resistivity relationships constructed from borehole logging data (black squares), individual inversions (green triangles), and joint inversion (blue dots).

the models. Overall, we achieve a good fit to the data, and only the long-period MT data are not matched very well by the models. Partially, this seems to be due to the fact that the impedance error estimates reported with the data are too low and actual errors are larger than the assumed error floor of 5%.

[18] Figure 3 shows the joint inversion model (bottom) and individual inversion results (top) along a transect below the seismic line. The joint inversion models show a signature of the salt dome in the form of a high-velocity, high-resistivity, and low-density anomaly, the expected signature for salt within sediments [e.g., *Panzner et al.*, 2011]. Compared to the individual inversion results, the velocity and density anomalies for the joint inversion are much more extensive. The resistivity anomaly is relatively similar in shape, but the maximum resistivity is substantially higher. These results demonstrate how the geometry of the resistivity anomaly is imprinted through structural coupling on the other two methods. This is particularly evident for the density model. For the inversion of gravity data alone, the low-density anomaly is concentrated near the surface, a feature often observed in gravity inversion [*Li and Oldenburg*, 1998], while in the joint inversion model, this anomaly is located significantly deeper.

[19] Comparison with a migrated seismic reflection profile [*Hokstad et al.*, 2011] shows that we achieve a good recovery of the geometry of the upper part of the salt dome. The regularization prevents a sharp transition between the background sediments and the highly anomalous salt in all models. Here, utilizing the seismic reflection data to modify the regularization could help to sharpen the images, and we will investigate this possibility in the future. With the current global regularization approach, these smooth models represent the best compromise between resolution and parameter variance [*Menke*, 1989]. Already, our joint inversion results produce a more consistent image of the salt structure than a comparison of the individual results, and the depth extent of the salt inferred from the joint inversion matches what is known from exploration activity at this location [*Hokstad et al.*, 2011].

[20] We can compare the relationship between velocity and resistivity in our models with logging measurements from two boreholes drilled into the flank of the salt dome. The plots of the logged velocities and conductivities along the borehole tracks in Figure 3 exhibit the same problem as the comparison with the seismic reflection data. While the boreholes show a sharp increase in velocity and decrease in resistivity coincident with the boundary of the salt dome, our inversion results change more gradually due to the imposed smoothness constraints. Still, we match the logging values for the surrounding sediments well, and the joint inversion reaches similar resistivities and velocities as the borehole in the center of the salt dome as permitted by the smoothing. Given the issues with smoothing in the inversion models, it is instructive to compare the inversion results with the logging data by displaying them in the form of a velocity-conductivity relationship as shown in Figure 4.

[21] Both individual inversion models and the joint inversion model approximate the relationship for the background sediments well. Between 2000 and 4000 m/s, they match not only the mean of the borehole values but also their variance. The logging data within the salt cluster around 4500 m/s and 500 Ωm, respectively. These values are only matched by the joint inversion results; the individual MT inversion exhibits lower resistivity values despite the fact that both misfit and roughness values for these models are comparable. From this perspective, the joint inversion results are superior to the individual inversion results. To some degree, the match between the logging relationship and the models is surprising though, as these values have been obtained on significantly different scales, a few centimeter for the borehole log and several hundred meters for the inversion. In this case, however, upscaling of the logging results does not appear to be a problem.

## 4. Conclusions

[22] Our results indicate how joint inversion can help to obtain more accurate images of complex geological structures and how we can reconstruct velocities-conductivity relationships from structural joint inversion approaches. Compared to individual inversion, we retrieve better the geometry and match the parameter relationship for the salt dome derived from borehole data. Considering the different length scale of the borehole logging data and the geophysical measurements on the surface, the match is somewhat surprising. It provides a strong argument for including borehole measurements into the joint inversion and further substantiates approaches that use parameter relationships derived from joint inversion for further analysis such as lithological classification [e.g., *Bedrosian*, 2007; *Doetsch et al.*, 2010; *Bauer et al.*, 2012].

[23] As we demonstrated on synthetic data [*Moorkamp et al.*, 2011], utilizing the information content of the borehole data has the potential to further improve our results. A particular issue in this case is the bimodal nature of the parameter relationship. While the relationship for the sediments can be described by a polynomial, the values for the salt cluster around a different value. We are currently working on methods to incorporate these types of relationships in the joint inversion approach.

[24] **Acknowledgments.** This work was funded by Chevron, ExxonMobil, Nexen, RWE Dea, Shell, Statoil, and Wintershall within the JIBA consortium. Thanks to Statoil for permission to use the real data.

[25] The Editor thanks two anonymous reviewers for their assistance in evaluating this paper.

## References


Abubakar, A., M. Li, Y. Lin, and T. Habashy (2012), Compressed implicit Jacobian scheme for elastic full-waveform inversion, *Geophys. J. Int.*, *189*(3), 1626–1634.

Avdeev, D., and A. Avdeeva (2009), 3D magnetotelluric inversion using a limited-memory quasi-Newton optimization, *Geophysics*, *74*(3), F45–F57, doi:10.1190/1.3114023.

Avdeev, D. B., A. V. Kuvshinov, O. V. Pankratov, and G. A. Newman (2002), Three-dimensional induction logging problems, part I: An integral equation solution and model comparisons, *Geophysics*, *67*, 413–426, doi:10.1190/1.1468601.

Bauer, K., G. Muñoz, and I. Moeck (2012), Pattern recognition and lithological interpretation of collocated seismic and magnetotelluric models using self-organizing maps, *Geophys. J. Int.*, *189*(2), 984–998.

Bedrosian, P. A. (2007), MT+, integrating magnetotellurics to determine earth structure, physical state, and processes, *Surv. Geophys.*, *28*(2-3), 121–167.

Carcione, J. M., B. Ursin, and J. I. Nordskag (2007), Cross-property relations between electrical conductivity and the seismic velocity of rocks, *Geophysics*, *72*(5), E193–E204, doi:10.1190/1.2762224.

De Stefano, M., F. Andreasi, S. Re, M. Virgilio, and F. Snyder (2011), Multiple-domain, simultaneous joint inversion of geophysical data with application to subsalt imaging, *Geophysics*, *76*(3), R69–R80.

Doetsch, J., N. Linde, I. Coscia, S. A. Greenhalgh, and A. G. Green (2010), Zonation for 3D aquifer characterization based on joint inversions of multimethod crosshole geophysical data, *Geophysics*, *75*(6), G53–G64, doi:10.1190/1.3496476.

Gallardo, L. A., and M. A. Meju (2003), Characterization of heterogeneous near-surface materials by joint 2D inversion of DC resistivity and seismic data, *Geophys. Res. Lett.*, *30*(13), 1658, doi:10.1029/2003GL017370.

Gallardo, L. A., and M. A. Meju (2004), Joint two-dimensional DC resistivity and seismic travel time inversion with cross-gradients constraints, *J. Geophys. Res.*, *109*, B03311, doi:10.1029/2003JB002716.

Gallardo, L. A., and M. A. Meju (2007), Joint two-dimensional cross-gradient imaging of magnetotelluric and seismic traveltime data for structural and lithological classification, *Geophys. J. Int.*, *169*, 1261–1272, doi:10.1111/j.1365-246X.2007.03366.x.

Hansen, P. C. (1992), Analysis of discrete ill-posed problems by means of the L-curve, *SIAM Rev.*, *34*(4), 561–580.

Heincke, B., M. Jegen, and R. Hobbs (2006), Joint inversion of MT, gravity and seismic data applied to sub-basalt imaging, *SEG Tech. Program Expanded Abstr.*, *25*(1), 784–789, doi:10.1190/1.2370374.

Heincke, B., H. Maurer, A. G. Green, H. Willenberg, T. Spillmann, and L. Burlini (2006), Characterizing an unstable mountain slope using shallow 2D and 3D seismic tomography, *Geophysics*, *71*, B241–B256, doi:10.1190/1.2338823.

Hokstad, K., et al. (2011), Joint imaging of geophysical data: Case history from the Nordkapp Basin, Barents Sea, *SEG Tech. Program Expanded Abstr.*, *30*(1), 1098–1102.

Jegen, M. D., R. W. Hobbs, P. Tarits, and A. Chave (2009), Joint inversion of marine magnetotelluric and gravity data incorporating seismic constraints: Preliminary results of sub-basalt imaging off the Faroe Shelf, *Earth Planet. Sci. Lett.*, *282*, 47–55, doi:10.1016/j.epsl.2009.02.018.

Lelièvre, P. G., C. G. Farquharson, and C. A. Hurich (2012), Joint inversion of seismic traveltimes and gravity data on unstructured grids with application to mineral exploration, *Geophysics*, *77*, K1–K15, doi:10.1190/geo2011-0154.1.

Li, Y., and D. W. Oldenburg (1998), 3-D inversion of gravity data, *Geophysics*, *63*, 109–119, doi:10.1190/1.1444302.

Linde, N., A. Tryggvason, J. E. Peterson, and S. S. Hubbard (2008), Joint inversion of crosshole radar and seismic traveltimes acquired at the South Oyster Bacterial Transport Site, *Geophysics*, *73*, G29–G37, doi:10.1190/1.2937467.

Menke, W. (1989), *Geophysical Data Analysis: Discrete Inverse Theory, Int. Geophys. Ser.*, vol. 45, 289 pp., Academic Press, New York.

Moorkamp, M., M. Jegen, A. Roberts, and R. Hobbs (2010), Massively parallel forward modeling of scalar and tensor gravimetry data, *Comput. Geosci.*, *36*(5), 680–686, doi:10.1016/j.cageo.2009.09.018.

Moorkamp, M., B. Heincke, M. Jegen, A. W. Roberts, and R. W. Hobbs (2011), A framework for 3-D joint inversion of MT, gravity and seismic refraction data, *Geophys. J. Int.*, *184*, 477–493, doi:10.1111/j.1365-246X.2010.04856.x.

Nagihara, S., and S. A. Hall (2001), Three-dimensional gravity inversion using simulated annealing: Constraints on the diapiric roots of allochthonous salt structures, *Geophysics*, *66*, 1438–1449, doi:10.1190/1.1487089.

Nocedal, J., and S. Wright (2006), *Numerical Optimization*, 2nd ed., 664 pp., Springer, New York.

Panzner, M., J. Ebbing, and M. Jordan (2011), 3D gravity inversion constrained by stereotomography, *SEG Tech. Program Expanded Abstr.*, *30*(1), 866–871.

Podvin, P., and I. Lecomte (1991), Finite difference computation of traveltimes in very contrasted velocity models: A massively parallel approach and its associated tools, *Geophys. J. Int.*, *105*, 271–284, doi:10.1111/j.1365-246X.1991.tb03461.x.

Vermeesch, P. M., J. V. Morgan, G. L. Christeson, P. J. Barton, and A. Surendra (2009), Three-dimensional joint inversion of traveltime and gravity data across the Chicxulub impact crater, *J. Geophys. Res.*, *114*, B02105, doi:10.1029/2008JB005776.